Comparison of Surface and Satellite-Derived Cloud and Radiation Properties at the Atmospheric Radiation Measurement Southern Great Plains and Tropical Western Pacific

M.L. Nordeen, M.M. Khaiyer, D.R. Doeling, and D. Phan
Analytical Services and Materials, Inc.
Hampton, Virginia

P. Minnis
NASA Langley Research Center
Hampton, Virginia

Introduction

Although the Atmospheric Radiation Measurement (ARM) program measurements of surface radiation budget can be found at the various cloud and radiation testbed sites, surface radiation data are needed over larger areas than represented by the surface radiometers. In order to provide surface radiative fluxes over the greater ARM domains, this study describes the implementation of radiative transfer algorithms to calculate surface fluxes from satellite cloud and radiance data retrieved with the visible infrared solar-infrared split window technique (VISST) algorithm (Minnis et al. 1995). The satellite-derived surface flux calculations are compared with ground-based instruments from the Southern Great Plains (SGP) Central Facility (CF), and the Tropical Western Pacific (TWP) sites of Manus, Nauru, and Darwin for validation purposes. When the flux retrieval accuracies are satisfactory, these satellite-based surface fluxes have the potential to constitute a new ARM value added product (VAP). In addition to validating surface fluxes, this study includes a section on VISST cloud property validation.

Data

The VISST algorithm analyzes 4-km cloudy pixels from the ninth Geostationary Operational Environmental Satellite (GOES-9) imager over the TWP domains (Phan et al. 2004) and from GOES-8 and GOES-10 over the SGP domains (Minnis et al. 2001). The pixels are identified as clear or cloudy using the Clouds and Earth's Radiant Energy System (CERES) ARM Cloud Mask (CACM; see Trepte et al. 2005). VISST-based top-of-atmosphere (TOA) shortwave (SW) and longwave (LW) fluxes were obtained by computing averages using all pixels within a 10-km radius of each surface site. The TOA fluxes were derived from the visible and infrared channels using the narrowband to broadband conversion functions found from matching CERES data with satellite data. The TOA fluxes over the SGP were derived from the visible and infrared channels using the narrowband to broadband conversion functions developed using matched CERES and GOES data (Doelling et al. 2003, Chakrapani et al. 2003). The conversion functions applied over the TWP used narrow-to-broadband

coefficients derived over ocean from GOES and CERES data taken over the ocean surrounding Florida in July 2002. Data from January, April, July, and October 2004 were used for the TWP sites and from April, July, and October 2004 and January 2005 for the SGP site. Several VISST parameters are used as input into three different algorithms to calculate surface fluxes at each of the CART sites. Profiles of temperature and humidity used in both the VISST and surface flux calculations are the hourly Rapid Update Cycle (RUC; Benjamin et al. 2004) profiles over the SGP and the 6-hourly Aviation (AVN) profiles over the TWP. Each vertical profile is temporally interpolated to match the GOES imager data for the relevant domain. Ozone, aerosol optical depth (AOD), and surface emissivity data are also needed for the satellite-derived surface flux calculations. The ozone data were obtained from the Total Ozone Mapping Spectrometer (TOMS) daily climatology ozone maps (McPeters 1998). AOD data were taken from the Geophysical Fluid Dynamics Laboratory (GFDL) climatology and are used to calculate aerosol correction parameters for the SW flux computations. Surface emissivity was obtained from CERES Moderate-Resolution Imaging Spectroradiometer analyses (Chen et al. 2004) and used to calculate LW upwelling flux.

One-minute Solar Infrared Radiation Station (SIRS) data, obtained from the *sgpsirs* files in the ARM archive, are used to validate the satellite-derived surface fluxes over the SGP. At the SGP CF, 10-minute means centered on the satellite image time were computed from 1-minute SIRS data. Over the TWP, the same process is used, except that the ARM groundrad (GRAD) and skyrad (SRAD) measurements replace the SIRS data. The TWP CART site ground radiometer b1 files (*twpgndrad60s* or *twpskyrad60s*) were obtained from the ARM archive. The *twpgndrad60s* files contain the upwelling SW and LW hemispheric irradiances from the pyranometer and pyrgeometer, respectively. The *twpskyrad60s* files contain the downwelling SW and LW hemispheric irradiances from the pyranometer and the shaded pyrgeometer1, respectively.

The cloud property validation datasets include retrievals from available ARM instruments at the SGP CF and TWP sites. The Active Remote Sensing of Clouds (ARSCL) derived cloud fraction and cloud top heights (Clothiaux et al. 2000) from 1998-2002 for SGP and April-December 2003 for the TWP are used for comparisons with satellite-derived cloud fraction and cloud top heights. Cloud fraction comparisons are also performed using the Total Sky Imager (TSI) from 2000-2002 over the SGP and April-December 2003 over the TWP. The CACM cloud fractions and VISST cloud heights were averaged over all pixels within a 20 km radius of the site and were compared with 20-minute averages of ARSCL cloud property data and TSI cloud fraction centered over each satellite's retrieval times. For the TSI data, averages are based on the "percent opaque" plus "percent thin" data within the 20-minute window with at least ten observations during that time. ARSCL cloud fraction is defined as the number of cloud occurrences divided by the total number of observations during the 20-minute time interval.

Methodologies and Results

Surface Radiation Validation

The Li-Leighton method is used to compute the net or absorbed surface SW flux in clear-sky conditions only (Li et al. 1993). This technique requires the following inputs: AOD, cosine of solar zenith angle (csza), preciptable water, and BB TOA SW albedo. The VISST cloud fraction is used to determine

clear-sky conditions. The maximum cloud fraction allowed for selecting clear-sky conditions is 5%. Li-Leighton estimates surface absorbed BBSW flux. Precipitable water is used to slightly modify the calculation of surface SW net flux.

The National Aeronautics and Space Administration (NASA) Langley Parameterized Shortwave Algorithm (LPSA) method is used to estimate surface SW downwelling flux under all-sky conditions (Gupta et al. 2001) and surface albedo in clear-sky conditions. This technique uses precipitable water, ozone, AOD, humidity profiles, csza, BB TOA clear-sky and cloud SW albedo, cloud fraction, and Earth Radiation Budget Experiment (ERBE) scene type. To compare the LPSA SW results with surface radiation measurements, the results are divided into clear-sky and cloudy conditions using the GOES cloud fraction. For clear-sky conditions, the GOES cloud fraction has to be less than or equal to 5% and cloudy conditions have a GOES cloud fraction greater than 5%.

The NASA Langley Parameterized Longwave Algorithm (LPLA) method is used for surface LW fluxes. The LPLA uses a set of parameterizations to estimate surface LW upwelling and downwelling fluxes under all-sky conditions (Gupta et al 1992). Inputs to this algorithm are liquid and ice cloud emissivity, cloud fraction, liquid and ice cloud base pressure, surface emissivity, and sounding profiles. As with SW surface flux results, the LW flux results are divided into clear-sky and cloudy conditions when comparing with surface radiation measurements based on the CACM cloud fraction.

Figure 1 shows the comparisons of Li-Leighton surface flux and SW net flux calculated obtained by adding GRAD and SRAD data together over Darwin. The satellite-based flux overestimates the instrument flux by an average of 32.9 Wm^{-2} or 6.1%. The outliers are probably the result of contamination of the observed scene by partly cloudy pixels that were classified as clear by the CACM. Darwin is located on a coast and the smaller surface albedo of the land-ocean combination observed from the GOES may account for the larger estimate of solar radiation absorption at the surface relative to the land-based ARM radiometers. On the other hand, the GOES narrowband-broadband calibration may not be optimal for this area.

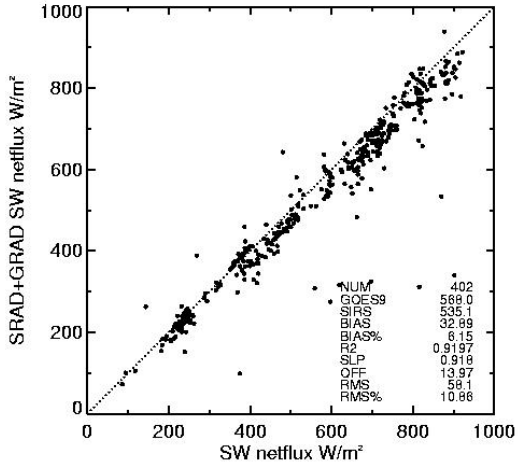

Figure 1. Comparison of Li-Leighton satellite-derived clear-sky SW net flux with ground instruments over Darwin for April, July, October 2004 and January 2005.

The LPSA derived clear-sky SW downwelling flux over Darwin underestimates the SRAD SW downwelling flux by an average of 2.7 Wm^{-2} or 0.4% with an root mean square (rms) error of 68.3 Wm^{-2} (Figure 2). Because the downwelling flux depends primarily on the atmospheric gas and aerosol profiles and less on the surface albedo or the satellite calibration, this unbiased clear-sky downwelling SW flux estimate is not surprising. Under cloudy conditions, the LPSA SW downwelling flux underestimates the SRAD SW downwelling flux by an average of 1.7 Wm^{-2} with an rms error of 168.5 Wm^{-2} (Figure 3). The scatter is quite large (32%) and is likely due to the frequent occurrence of mixtures of convective clouds with a variety of vertical structures that cause a deviation from the plane-parallel radiative transfer assumed in the parameterizations. The unbiased mean suggests that the input cloud properties provide an accurate measure of the cloud radiative characteristics.

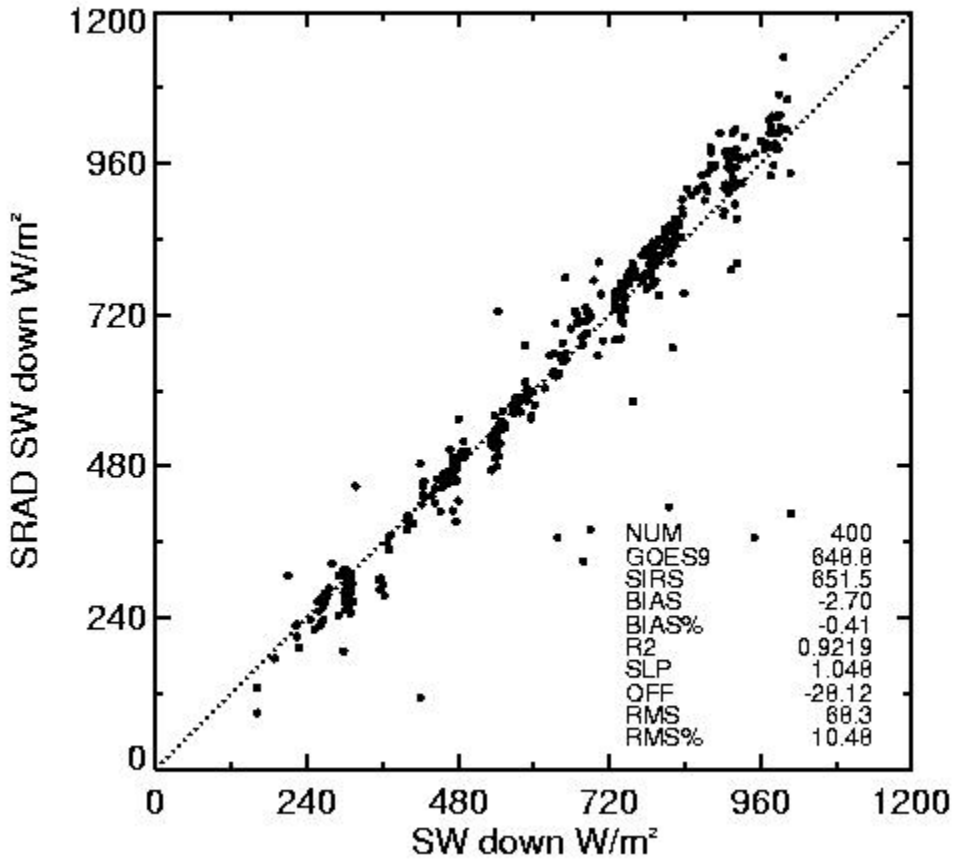

Figure 2. Comparison of satellite-derived SW downwelling flux from LPSA with SW downwelling surface flux over Darwin under clear-sky conditions.

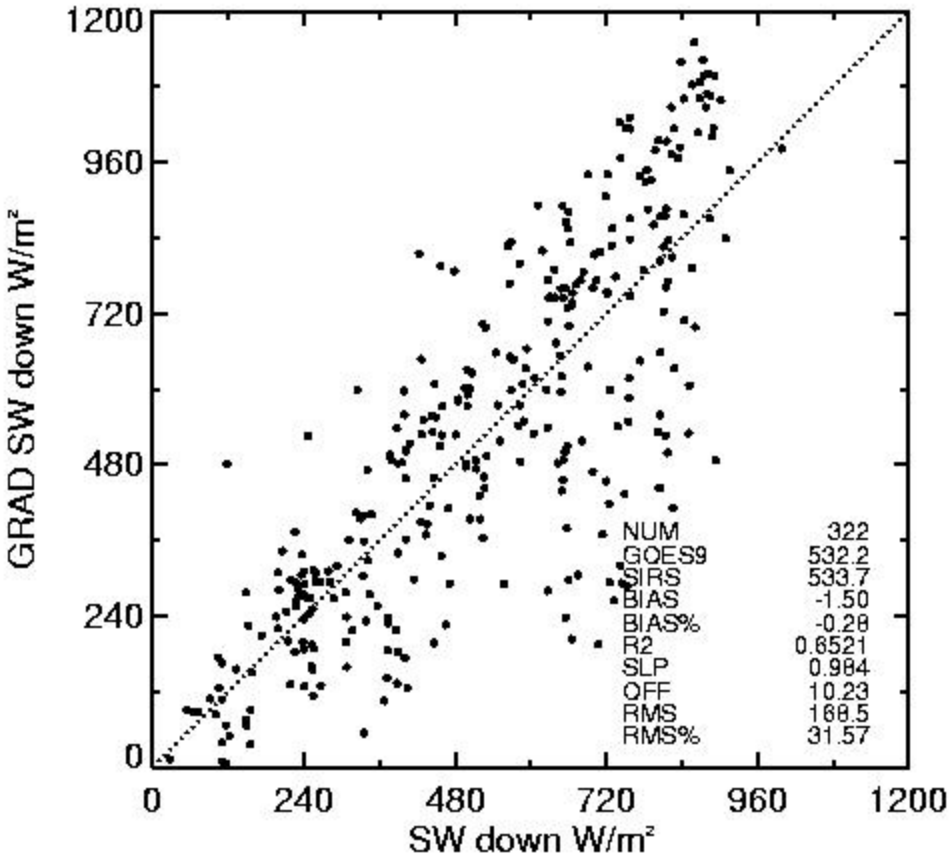

Figure 3. SW downwelling flux from GRAD and LPSA during cloudy conditions over Darwin.

Table 1 summarizes the results of the satellite-derived surface flux comparisons with surface data over all of the CART sites. A positive bias indicates that the satellite-derived surface flux overestimates the observed flux and a negative bias indicates underestimation. The Li-Leighton (LI) method performs best over the SGP with a bias of only -7.7 Wm^{-2}. The biases are much larger over the TWP sites, especially over Manus and Nauru. The lack of clear-sky conditions, only 74 cases at Nauru and 63 cases at Manus, over both of these sites could be hindering the calculations. It is possible that even the clear-sky conditions that were observed may still be contaminated by some cloudiness. The coastal effects on the GOES net SW flux estimate discussed for Darwin could be even worse for Manus and Nauru especially because of the increased percentage of water surface in the satellite data for the island sites. This coastal effect would not be operative at the SGP and could explain why the LI method yields only a small bias there.

Table 1. Summary of differences in surface fluxes derived from satellite and ground-based instruments over the CART sites. Li-Leighton method is shortened to LI for the table. LPSA is abbreviated as LS and LPLA is abbreviated as LL. Clear-sky conditions are shortened to clr and cld represents cloudy conditions. The abbreviations ddw, dup, ndw, and nup represent daytime LW downwelling, daytime LW upwelling, night-timeLW downwelling, and night-time LW upwelling, respectively.

a)	**SGP**			**DARWIN**		
	BIAS (Wm^{-2})	**RMS (Wm^{-2})**	**RMS (%)**	**BIAS (Wm^{-2})**	**RMS (Wm^{-2})**	**RMS (%)**
LI (clr)	-7.7	36.3	7.9	32.9	58.1	10.9
LS (clr)	-1.3	50.5	8.7	-2.7	68.3	10.5
LS (cld)	-6.6	93.8	25.4	-1.5	168.5	31.6
LL ddw clr	2.0	11.8	3.1	-13.7	10.6	2.7
LL ddw cld	16.6	14.9	4.0	-2.2	13.3	3.2
LL dup clr	-6.17	13.5	2.8	-65.0	26.8	5.0
LL dup cld	-7.0	16.0	3.6	-44.2	27.3	5.3
LL ndw clr	2.0	13.2	3.7	-9.9	9.8	2.5
LL ndw cld	7.1	15.9	4.4	20.4	31.3	8.0
LL nup clr	16.6	6.6	1.5	-10.2	6.3	1.3
LL nup cld	12.1	5.5	1.3	0.9	9.0	2.0
b)	**MANUS**			**NAURU**		
	BIAS (Wm^{-2})	**RMS (Wm^{-2})**	**RMS (%)**	**BIAS (Wm^{-2})**	**RMS (Wm^{-2})**	**RMS (%)**
LI (clr)	67.9	72.5	13.0	125.8	131.9	26.1
LS (clr)	-16.3	69.8	14.3	12.7	113.3	31.1
LS (cld)	39.1	158.7	41.6	17.9	161.5	38.5
LL ddw clr	5.67	8.1	2.0	-1.1	10.9	2.6
LL ddw cld	17.6	9.5	2.2	10.0	10.4	2.4
LL dup clr	-45.1	26.2	5.1	-25.0	17.5	3.5
LL dup cld	-18.0	24.6	5.1	-14.8	19.7	4.1
LL ndw clr	15.0	10.7	2.6	10.2	7.5	1.8
LL ndw cld	20.3	10.2	2.5	11.8	9.2	2.2
LL nup clr	20.1	11.5	2.6	24.5	6.6	1.5
LL nup cld	20.5	7.1	1.6	19.5	6.6	1.5

The LPSA clear-sky SW downwelling fluxes are more accurate than the LI fluxes at all four sites with biases less than +3.5% at all locations. The LPSA biases for cloudy conditions range from -1.7 to 10.3% while the rms errors are 34.3% for all four sites. The smallest rms difference is found over the SGP and may be the result of having stratiform clouds occurring more frequently there than over any of the TWP sites. The larger rms errors at Manus and Nauru could also be due to the large surface albedo differences between land and ocean. Additional study is needed to confidently explain the sources of the regional differences in the bias and rms errors. Nevertheless, the relatively small bias errors are encouraging; they suggest that the cloud properties are efficacious in producing the correct surface SW fluxes, on average.

Under daytime clear-sky conditions, the LW downwelling satellite-derived surface fluxes over Darwin are biased by -13.7 Wm^{-2} with an rms error of 10.6 Wm^{-2} (Figure 4) while daytime cloudy conditions produce a bias of -2.2 Wm^{-2} or 0.5% with an rms error of 13.3 Wm^{-2} (Figure 5).

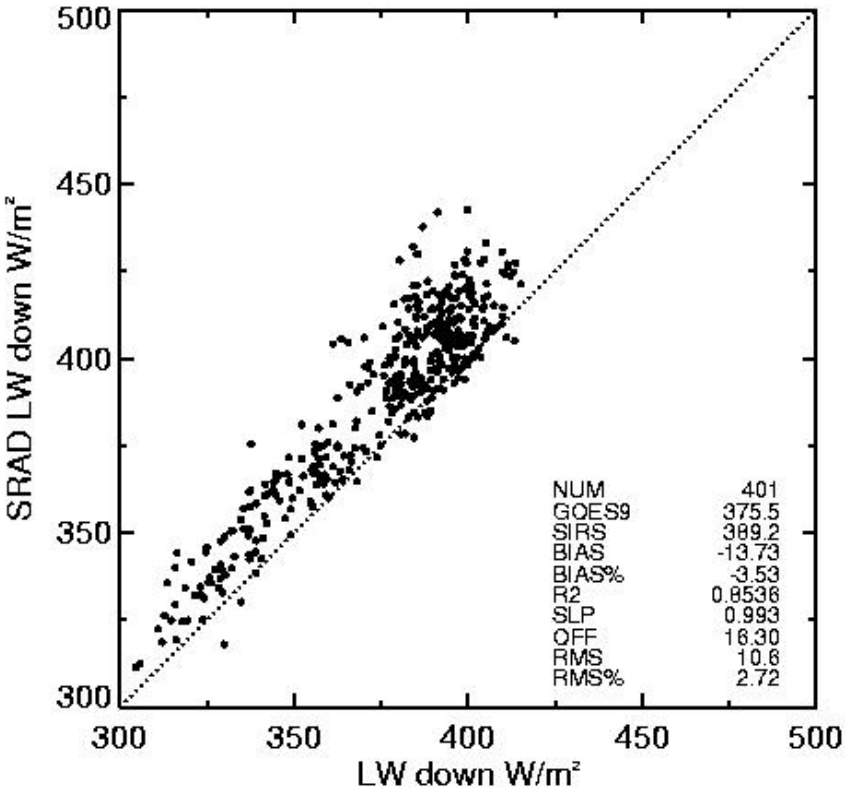

Figure 4. Downwelling LW from SRAD and LPLA under clear-sky conditions over Darwin.

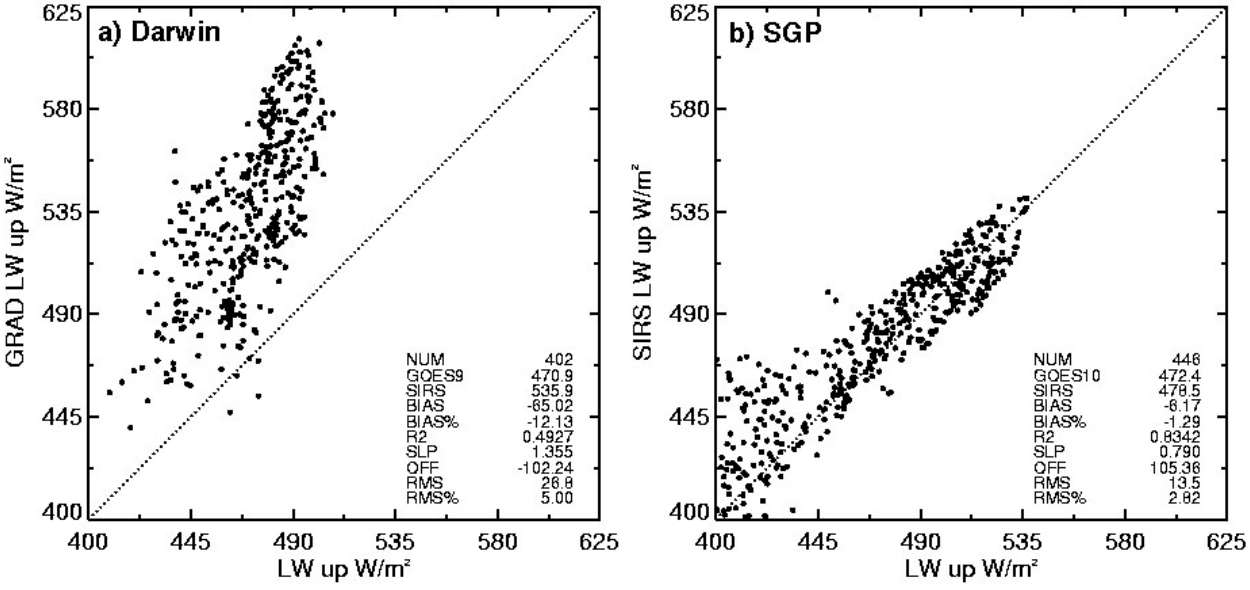

Figure 5. Downwelling LW from SRAD and LPLA under cloudy conditions over Darwin.

The calculated LW upwelling fluxes for clear-skies over Darwin (Figure 6a) suggest that the surface skin temperature input into the algorithm is probably too small, perhaps due to the coastal effect, which would decrease the average daytime LW flux and suppress the diurnal temperature range seen by the satellite. That could explain why GRAD LW flux varies by almost 150 Wm^{-2} compared to only 100 Wm^{-2} estimated from the satellite data. At night (not shown), the dynamic range is the same for both datasets, but the GOES estimate is too low by 2.1%.

The daytime clear-sky upwelling LW biases are much smaller and the dynamic range is the same for both datasets over the SGP (Figure 6b). There, the ocean-land contrast is not a factor. The scatter is relatively small (< ± 15 Wm^{-2}) at the high end (flux > 470 Wm^{-2}) of the range, but is much greater at the low end. The GOES flux estimates are also unbiased at the high end of the range but are too small at the lower extreme. This difference suggest that some residual cloud cover, perhaps, thin cirrus clouds was missed by the CACM or the surface emissivity was improperly characterized due to precipitation or vegetation changes that were not included in the relatively static emissivity maps. At night (not shown), the GOES-based upwelling clear-sky LW fluxes are too large by 3.8%, on average, but very well correlated with the SIRS fluxes. The standard deviation of the differences is only 1.5%. This offset between the two datasets could be the result of biases in surface emissivity biases, spatial variability (the CF is not representative of the 10-km radius?), the surface instrument, or the parameterizations.

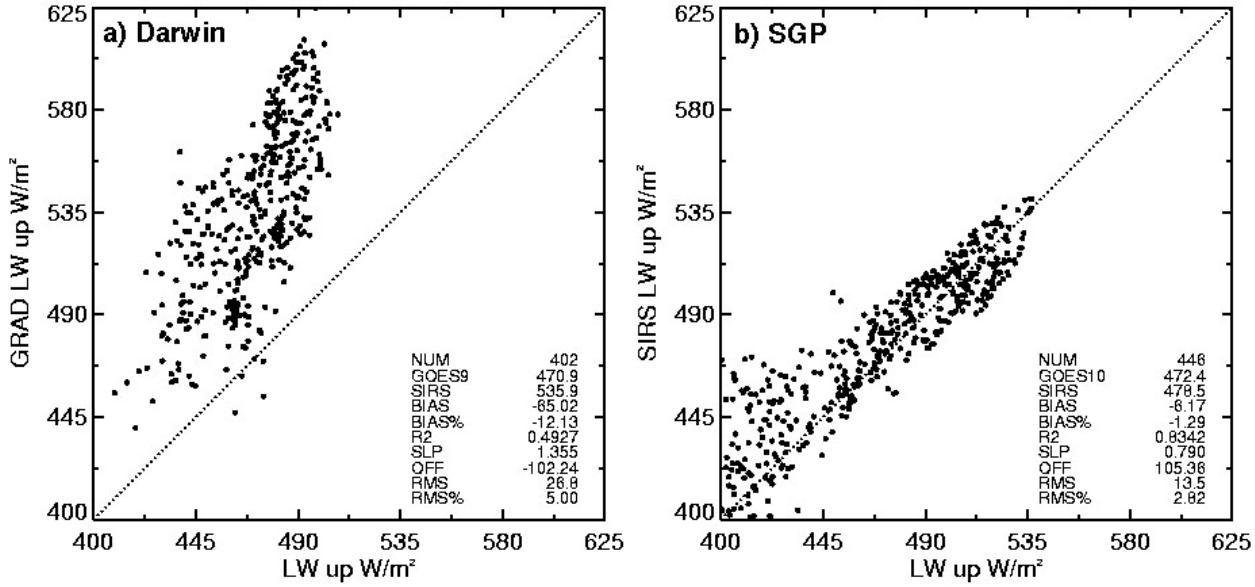

Figure 6. a) Upwelling LW clear-sky fluxes from GRAD and LPLA over Darwin. b) Upwelling LW clear-sky fluxes from SIRS and LPLA over SGP.

During cloudy conditions, the numerical weather analysis surface air temperatures are used as estimates of the skin temperature. Over Darwin, this does not appear to be a good assumption because the upwelling LW flux is underestimated by 44 Wm^{-2} (Figure 7a) and the dynamic range is compressed by 100 Wm^{-2}. The spatial and temporal resolution of the AVN is apparently too low to capture the dynamic range and may be overly influenced by the sea surface temperature. The RUC provides a better basis for using the surface air temperature because it has high spatial and temporal resolution resulting in a much

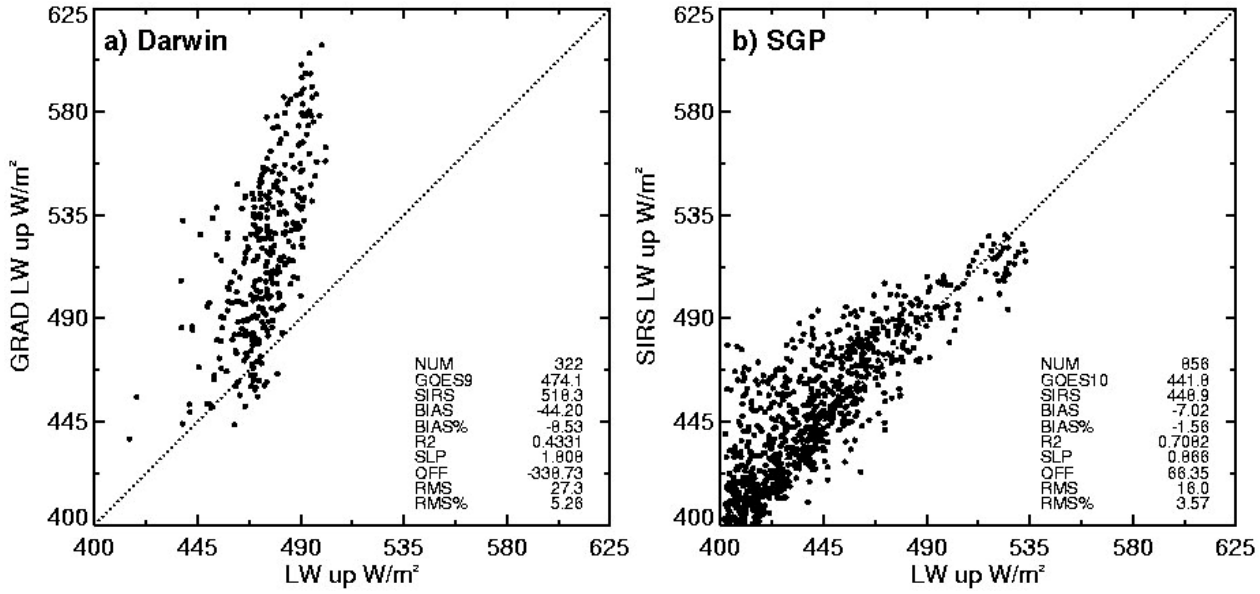

Figure 7. a) Upwelling LW fluxes from GRAD and LPLA over Darwin for cloudy conditions. b) Upwelling LW fluxes from SIRS and LPLA over SGP for cloudy conditions.

smaller bias and rms errors (Figure 7b). The larger scatter at the low end of the range could be due to an optical depth effect that is not included in the use of the air temperature as a substitute for skin temperature. When the clouds are optically thin, the surface may undergo solar heating that could cause an offset between the air and skin temperatures resulting in the scatter seen in Figure 7b.

In Table 1, the daytime clear-sky downwelling LW flux biases range from -3.5% to 1.4% while the rms errors are 10.4%. Since downwelling LW clear-sky flux is a function of the 800-1000 mb temperature and humidity profile, the range in the TWP biases could result from the errors in the AVN profiles peculiar to each site. Differences in each site' bias could also be a result of possible cloud contamination in the clear-sky mask at each site. Under daytime cloudy conditions, the biases range from -0.5 to 4.5%. In addition to the profile, the cloudy downwelling LW flux depends on the cloud base pressure derived from the parameterization of Chakrapani et al. (2002). Since cloud base pressure is based on calculations of cloud thickness parameters over the SGP and might not truly represent cloud thicknesses over the TWP, they could cause biases in the LW estimates.

For the daytime upwelling LW fluxes, the clear-sky flux bias ranges from -12.1% to –1.3% while the cloudy flux bias ranges between -8.5% to –1.6%. The main problem with the upwelling LW calculations over the TWP sites appears to be that the profiles are more representative of the ocean instead of the coastal TWP sites. This causes the profiles to miss the diurnal cycle and other land-ocean interactions over the TWP resulting in smaller upwelling flux calculations during the day and larger values during the night.

Cloud Property Validation

Individual GOES 20-km radius cloud fractions and the 20-minute averaged daytime cloud amounts derived from TSI and ARSCL over the SGP are compared sorting the matched pairs into pairs of cloud fraction intervals: 0-20%, 20-50%, 50-80%, and 80-100%. The percentage values found along the diagonal indicate how well each method agrees with the others. Table 2a reveals that over the SGP, ARSCL and CACM agree in 72% of all daytime cases while the TSI and CACM cloud amounts are in agreement 74% of the time (Table 2b). In Table 2a, 14% of the results are separated by two or more bins. Only 8% of the TSI-CACM matches are separated by two or three bins. The largest difference, 6%, is found for nearly clear ARSCL and overcast CACM matches. This discrepancy is unlikely and could be due to misclassification of heavily precipitating systems as clear-sky conditions. This large difference is not found for the TSI-CACM comparison.

Table 2. a) Daytime cloud fractions from ARSCL and CACM over SGP. b) Daytime cloud fractions from TSI and CACM over the SGP. Each number represents the percentage of cases found in each bin.

2a)

		0-20%	20-50%	50-80%	80-100%
ARSCL	80-100%	1	2	3	32
	50-80%	1	1	1	2
	20-50%	2	1	1	2
	0-20%	38	4	2	6
		CACM			

2b)

		0-20%	20-50%	50-80%	80-100%
TSI	80-100%	1	1	2	32
	50-80%	3	2	2	4
	20-50%	8	3	2	1
	0-20%	37	2	1	1
		CACM			

Table 3 shows statistical summaries of the comparisons. The CACM underestimates cloud fraction by 4% relative to the TSI, but overestimates cloud amount relative to the ARSCL results. The rms differences between the CACM and TSI are 10% smaller than those between the ARSCL and the two other methods. The CACM and TSI both measure much larger areas than the nearly point measurement made by the active surface instruments.

Table 3. Mean daytime cloud amounts for each instrument over the SGP.

	NCASES	TSI (%)	CACM (%)	ARSCL (%)	BIAS (%)	RMS
TSI/CACM	14393	48.2	44.2		-4.0	22.3
ARSCL/CACM	27258		49.8	43.8	6	32.3
ARSCL/TSI	13284	51.4		41.9	-9.5	33.5

Similar comparisons were performed using daytime data from Nauru. The ARSCL and CACM cloud amounts agree in only 53% of the cases while the TSI and CACM agree in 57% of the cases. The CACM and ARSCL results differ by 2 or 3 categories in 25% of the cases. The TSI and CACM have significant differences in only 7% of cases, a value similar to that over the SGP. For the matched sets,

the ARSCL and TSI return 5 and 6% more cloud cover than the CACM (Table 5), while the ARSCL yields 7% less cloud cover than the ARSCL. These differences may be attributable to island effects that could bias the surface-based cloud amounts at Nauru. A cloud plume frequently extends westward from Nauru (Nordeen et al. 2001) and may be often be detected by the ARSCL sensors and nearly always by the TSI. The TSI is able to detect clear skies more often because its view can include more than the plume when it extends over the site. This evident in the differences in overcast cases in Table 4, where the TSI and ARSCL find overcast conditions 24 and 33% of the time, respectively. The satellite finds even less cloud cover because the persistent plume constitutes less of the total cover over the large area viewed by the satellite compared to that seen by the TSI.

Table 4. a) Daytime matched cloud fractions from ARSCL and CACM over Nauru. b) Daytime matched cloud fractions from TSI and CACM over Nauru.

4a)

		0-20%	20-50%	50-80%	80-100%
ARSCL	80-100%	4	4	5	20
	50-80%	5	2	2	3
	20-50%	10	3	2	2
	0-20%	28	4	2	4
		CACM			

4b)

		0-20%	20-50%	50-80%	80-100%
TSI	80-100%	0	0	2	22
	50-80%	4	3	4	6
	20-50%	19	7	4	2
	0-20%	24	2	1	0
		CACM			

Table 5. Mean daytime cloud amounts for each instrument over Nauru.

	NCASES	TSI (%)	CACM (%)	ARSCL (%)	BIAS (%)	RMS
TSI/CACM	1524	47.3	41.9		-5.4	23.9
ARSCL/CACM	1658		41.0	47.1	-6.1	38.6
ARSCL/TSI	687	37.5		44.8	7.3	34.2

Cloud heights were compared by first classifying each surface-satellite pair by the ARSCL-determined single layer cloud height: low clouds (ARSCL < 4 km), mid-level clouds (4 km < ARSCL <7.5 km), and high clouds (ARSCL > 7.5 km). Only cases where the daytime CACM-derived cloud fraction is greater than 90% are used here. Further classifications were made using ARSCL derived cloud thicknesses (dz) and categorizing GOES clouds as either liquid or ice. If VISST classifies at least 90% of the cloudy pixels as liquid, the cloud is classified as liquid. A similar approach is used to define ice clouds.

Over the SGP, the VISST and ARSCL cloud top heights in Table 6 are in relatively good agreement for both low liquid and high ice cloud cases. The VISST overestimates cloud top height by 0.3 km for thinner clouds and underestimates cloud tops in medium and thick liquid cases by 0.5 km. For high clouds, VISST underestimates cloud top height for all thickness levels with medium thick ice clouds having the largest bias of -1.2 km.

Table 6. Daytime cloud top heights (ztop) over the SGP for low liquid and high ice clouds.

	liq 0<dz<1.5	liq 1.5<dz<3.5	liq dz > 3.5	ice 0<dz<1.5	ice 1.5<dz<3.5	ice dz > 3.5
ncases	667	399	13	135	792	1209
ARSCL ztop(km)	1.54	2.58	3.80	10.73	10.61	10.46
VISST ztop (km)	1.83	2.12	3.19	9.76	9.43	9.70
Bias ztop (km)	0.29	-0.46	-0.61	-0.97	-1.18	-0.77
RMS ztop	0.83	1.00	1.00	2.43	1.80	1.28

Over Nauru (Table 7), the VISST high cloud top comparisons are in excellent agreement for the thin and medium thickness cloud, but are underestimated by 1.3 km for thick high clouds. This persistent bias for thick clouds, where agreement would seem to be a given, is a common problem in deep tropical systems (e.g., Sherwood et al. 2004). The VISST overestimates the height of the thin liquid clouds by 1.4 km. It is not clear, at this point, if there is any sort of island effect in the cloud heights or whether the VISST is overcorrecting for low-cloud semi-transparency or is affected by partially cloud-filled pixels.

Table 7. Daytime cloud top heights (ztop) over Nauru for low liquid and high ice clouds.

	liq 0<dz<1.5	ice 0<dz<1.5	ice 1.5<dz<3.5	ice dz > 3.5
ncases	2	33	11	2
ARSCL ztop (km)	2.18	11.68	11.75	12.92
VISST ztop (km)	3.53	11.84	11.58	11.61
Bias ztop (km)	1.36	0.15	-0.16	-1.31
RMS ztop	1.47	1.25	1.98	1.34

Summary and Future Work

The surface flux results are preliminary, but show good agreement over Darwin and SGP. Some of the scatter in the clear-sky results is due to cloud contamination in the clear-sky classifications. Possible solutions to some of the discrepancies found in the TWP surface flux results are the future use of a new narrowband-to-broadband flux fits and the use of higher temporal resolution profile data over the TWP. The coastal effects need to be investigated more closely to determine how much of the bias or dynamic range is due to water-land differences.

The cloud property validation results revealed a site and instrument dependency in the cloud fraction results. Different environments and air mass types could explain some of the site dependency, but over Nauru, island effects could be a large source of errors. VISST could also be missing or overestimating cloud fractions by misclassifying partially filled pixels as completely clear or cloudy. Satellite-derived cloud heights generally compared well with ARSCL-derived heights if the cloud phase was correctly determined by VISST, except for thin low clouds over Nauru. The influence of partially cloud-filled pixels, island effects, and vertical temperature profiles need to be examined in more detail.

Acknowledgements

This research was supported by the Environmental Sciences Division of the U.S. Department of Energy Interagency Agreement DE-AI02-97ER62341.

Corresponding Author

Michele L. Nordeen, m.l.nordeen@larc.nasa.gov, (757) 827-4640

References

Benjamin, SG, D Dévényi, SS Weygandt, KJ Brundage, JM Brown, GA Grell, D Kim, BE Schwartz, TG Smirnova, TL Smith, GS Manikin. 2004 "An hourly assimilation-forecast cycle: The RUC." *Monthly Weather Review* 132, 495-518.

Chen, Y, S Sun-Mack, P Minnis, DF Young, and WL Smith, Jr. 2004. "Seasonal surface spectral emissivity derived from Terra MODIS data." In *Proceedings of the Thirteenth AMS Conference Satellite Oceanography and Meteorology*, Norfolk, Virginia, September 20-24, CD-ROM, P2.4.

Chakrapani, V, DR Doelling, AD Rapp, and P. Minnis. 2002. "Cloud Thickness Estimation from GOES-8 Satellite Data Over the ARM-SGP Site." In *Proceedings of the Of Twelfth Annual ARM Science Team Meeting*, St. Petersburg, Florida, April 8-12.

Chakrapani V, DR Doelling, MM Khaiyer, and P Minnis. 2003. "New Visible to Broadband Shortwave Conversions for Deriving Albedos from GOES-8 Over the ARM SGP." In *Proceedings of the Thirteenth Annual ARM Science Team Meeting*, Boulder, Colorado, March 31-April 4.

Clothiaux, EE, TP Ackerman, GG Mace, KP Morgan, RT Marchand, M Miller, and BE Martner. 2000. "Objective determination of cloud heights and radar reflectivities using a combination of active remote sensors at the ARM CART sites." *Journal of Applied Meteorology* 39, 645-665.

Doelling, DR, MM Khaiyer, and P Minnis. 2003. "Improved ARM-SGP TOA OLR Fluxes from GOES-8 IR Radiances based on CERES data." In *Proceedings of the Thirteenth Annual ARM Science Team Meeting*, Boulder, Colorado, March 31-April 4.

Gupta, SK, WL Darnell, and AC Wilber. 1992. "A Parameterization for Longwave Surface Radiation from Satellite Data: Recent Improvements." *Journal of Applied Meteorology* 31, 1361-1367

Gupta, SK, DP Kratz, PW Stackhouse, Jr., and AC Wilber. 2001. The Langley Parameterized Shortwave Algorithm (LPSA) for Surface Radiation Budget Studies---Version 1.0, NASA/TP-2001-211272, p. 26

Li, Z, HG Leighton, K Masuda, and T Takashima. 1993. "Estimation of SW Flux Absorbed at the Surface from TOA Reflected Flux." *Journal of Climate* 6, 317-330.

Long, CN and JJ DeLuisi. 1998. "Development of an Automated Hemispheric Sky Imager for Cloud Fraction Retrievals." In *Proceedings of the Tenth Symposium on Meteorological Observations and Instrumentation*, Phoenix, Arizona, Jan. 11-16.

McPeters, RD, PK Bhartia, AJ Krueger, JR Herman, CG Wellemeyer, CJ Seftor, G Jaross, O Torres, L Moy, G Lavow, W Byerly, SL Taylor, T Swissler, and RP Cebula. 1998. Earth Probe Total Ozone Mapping Spectrometer (TOMS) Data Products User's Guide. NASA Reference Publication 1998-206895

Minnis, P. and National Aeronautics and Space Administration. 1995. Cloud Optical Property Retrieval (Subsystem 4.3). In Clouds and the Earth's Radiant Energy System (CERES) Algorithm Theoretical Basis Document, Vol. III: Cloud Analyses and Radiance Inversions (Subsystem 4), NASA RP 1376 Vol. 3, edited by CERES Science Team, pp. 135-176.

Minnis, P, WL Smith, Jr., DF Young, L Nguyen, AD Rapp, PW Heck, S Sun-Mack, QZ Trepte, and Y Chen. 2001. "A near-real time method for deriving cloud and radiation properties from satellites for weather and climate studies." In *Proceedings AMS Eleventh Conference Satellite Meteorology and Oceanography*, Madison, Wisconsin, October 15-18, pp. 477-480.

Nordeen, ML, P Minnis, DR Doelling, D Pethick, and L Nguyen. 2001. "Satellite observations of cloud plumes generated by Nauru." *Geophysical Research Letters* 28, 631-634.

Phan, D, DA Spangenberg, R Palikonda, MM Khaiyer, ML Nordeen, L Nguyen, and P Minnis. 2004. "Web-based satellite products database for meteorological and climate applications." In *Proceedings of the Thirteenth AMS Conference Satellite Oceanography and Meteorology*, Norfolk, Virginia, September 20-24, CD-ROM, P8.2.

Sherwood, SC, J-H Chae, P Minnis, and M McGill. 2004. "Underestimation of deep convective cloud tops by thermal imagery." *Geophysical Research Letters* 31 (11), 10.1029/2004GL019699.

Trepte, QZ, P Minnis, PW Heck, and R Palikonda. 2005. "Improvements in near-terminator and nocturnal cloud masks using satellite imager data over the ARM sites." In *Proceedings of the Fifteen ARM Science Team Meeting*, Daytona Beach, Florida, March 14-18.